

A levitation instrument for containerless study of molten materials

Paul C. Nordine, Dennis Merkley, Jeffrey Sickel, Steve Finkelman, Rainer Telle et al.

Citation: *Rev. Sci. Instrum.* **83**, 125107 (2012); doi: 10.1063/1.4770125

View online: <http://dx.doi.org/10.1063/1.4770125>

View Table of Contents: <http://rsi.aip.org/resource/1/RSINAK/v83/i12>

Published by the [American Institute of Physics](#).

Related Articles

Acoustic levitation with self-adaptive flexible reflectors
Rev. Sci. Instrum. **82**, 074904 (2011)

Acoustic wave levitation: Handling of components
J. Appl. Phys. **109**, 124901 (2011)

Nonlinear restoring forces and geometry influence on stability in near-field acoustic levitation
J. Appl. Phys. **109**, 084518 (2011)

Influence of gas inertia and edge effect on squeeze film in near field acoustic levitation
Appl. Phys. Lett. **96**, 243507 (2010)

Temperature dependence of single-axis acoustic levitation
J. Appl. Phys. **93**, 3016 (2003)

Additional information on *Rev. Sci. Instrum.*

Journal Homepage: <http://rsi.aip.org>

Journal Information: http://rsi.aip.org/about/about_the_journal

Top downloads: http://rsi.aip.org/features/most_downloaded

Information for Authors: <http://rsi.aip.org/authors>

ADVERTISEMENT

JANIS Does your research require low temperatures? Contact Janis today.
Our engineers will assist you in choosing the best system for your application.



10 mK to 800 K LHe/LN₂ Cryostats
Cryocoolers Magnet Systems
Dilution Refrigerator Systems
Micro-manipulated Probe Stations

sales@janis.com www.janis.com
Click to view our product web page.

A levitation instrument for containerless study of molten materials

Paul C. Nordine,^{1,a)} Dennis Merkley,¹ Jeffrey Sickel,² Steve Finkelman,¹ Rainer Telle,³ Arno Kaiser,³ and Robert Prieler³

¹Physical Property Measurements, Inc., 825 Chicago Avenue, Suite E, Evanston, Illinois 60202, USA

²Corpus Callosum Corporation, Evanston, Illinois 60202, USA

³Institut fuer Gesteinshuettenkunde/Mineral Engineering, RWTH Aachen University, Aachen, Germany

(Received 24 October 2012; accepted 21 November 2012; published online 14 December 2012)

A new aero-acoustic levitation instrument (AAL) has been installed at the Institute for Mineral Engineering at RWTH University in Aachen, Germany. The AAL employs acoustically stabilized gas jet levitation with laser-beam heating and melting to create a contact-free containerless environment for high temperature materials research. Contamination-free study of liquids is possible at temperatures in excess of 3000 °C and of undercooled liquids at temperatures far below the melting point. Digital control technology advances the art of containerless experiments to obtain long-term levitation stability, allowing new experiments in extreme temperature materials research and to study operation of the levitation instrument itself. Experiments with liquid Al₂O₃ at temperatures more than 3200 °C, 1200 °C above the melting point, and with liquid Y₃Al₅O₁₂ far below the melting point are reported. Fast pyrometry and video recording instruments yield crystallization rates in undercooled liquid Al₂O₃ as a function of temperature. Levitation of dense liquid HfO₂ at temperatures above 2900 °C is demonstrated. Capabilities are described for resonant frequency matching in the three-axis acoustic positioning system, acoustic control of sample spin, and position control of standing wave nodes to stabilize levitation under changing experimental conditions. Further development and application of the levitation technology is discussed based on the results of experiments and modeling of instrument operations. © 2012 American Institute of Physics. [<http://dx.doi.org/10.1063/1.4770125>]

I. INTRODUCTION

Aero-acoustic levitation (AAL) is a tool for experimental materials research at very high temperatures. Any sufficiently involatile materials can be levitated, laser-beam heated, and melted. Highly localized acoustic forces produced by standing waves stabilize levitation of samples that are supported by the aerodynamic drag force from a vertically flowing gas jet. At the same time, laminar gas jet flow eliminates turbulent natural convection in the sound field and keeps the acoustic forces stable when a levitated sample is heated and melted.

The AAL method^{1,2} was first described in 1994 and has since been used for a wide variety of high temperature processing and materials property research. Among its applications are glass³ and glass fiber⁴ synthesis, deep undercooling of oxide liquids,⁵⁻⁷ crystallization of metastable phases from undercooled liquids,⁶ contamination-free liquid-phase processing of ceramic superconductor materials,⁷ purification⁸ of molten Al₂O₃ by evaporation of residual Cr, splat-quenching of molten oxides,⁹ and controlled oxidation of Fe²⁺ in an alumino-silicate melt.¹⁰ The applications of AAL technology have emphasized materials processing experiments. Liquid property measurements are also possible and will benefit from the improved levitation stability and control that the present work achieves. In this paper we describe advances in the design and performance of the instrument, experiments in extreme temperature materials research, and studies of the instrument operation itself.

II. EXPERIMENTAL

A. Levitator description

A photograph of the aero-acoustic levitator is given in Figure 1. Components of the levitator are identified in the figure caption. Electronics, power supplies, communication devices, and the gas flow controller are mounted in the system frame. Two video cameras mounted on the AAL frame and a video monitor provide sample viewing during sample insertion and in manual control of the gas flow rate to maintain levitation at the intersection of the heating laser beams.

Experiments typically employ two operators. One operator at the computer controls sets acoustic power level, adjusts sample position feedback parameters that stabilize levitation, and controls the heating laser power. The second operator works at the apparatus to insert samples to initiate levitation, manually adjust gas flow rates, and terminate or restart laser heating with the laser kill switch.

The levitator has three sets of opposed acoustic transducers mounted on orthogonal axes. The bottom three acoustic transducers are labeled XA, YA, ZA and the top transducers are XB, YB, ZB, with XB located just above the Infinity lens, item 9 in Figure 1. Foam structures on the center area of each horn reduce the intensity of reflected sound waves from the opposite transducer.

The transducers are highly resonant devices with 38 ± 2 Hz bandwidths near 22 200 Hz. They have piezoelectric motors driven by Techron Model LV 3620 acoustic amplifiers in response to computer-controlled digital signal generator signals that determine the acoustic phase, frequency, and amplitude. Control electronics monitor the voltage, current,

^{a)} Author to whom correspondence should be addressed. Electronic mail: pnordine@ppmeasurements.com.

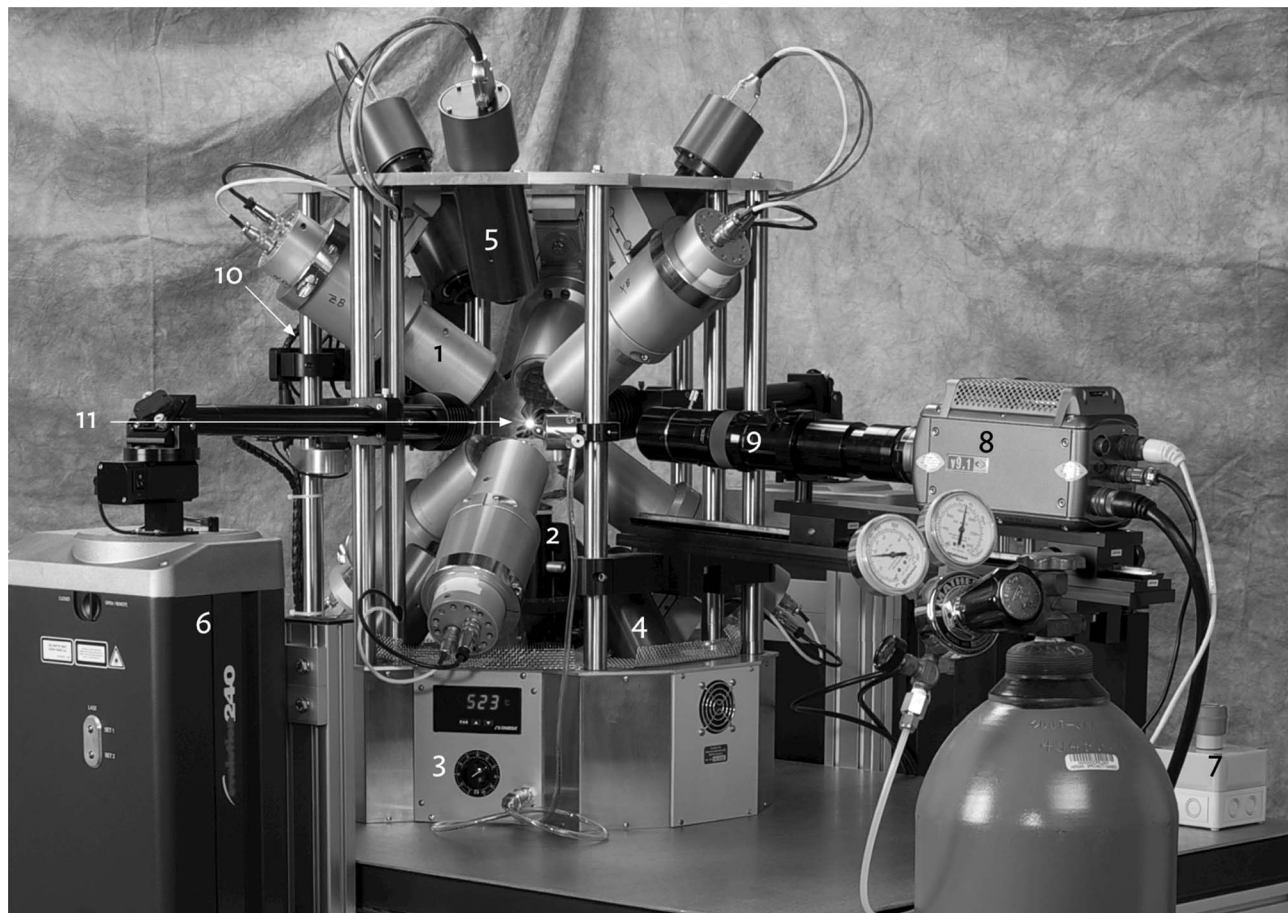


FIG. 1. Aero-acoustic levitator. 1—six acoustic transducers; 2—gas jet assembly; 3—gas jet heater control; 4—three diode laser sources for position sensing; 5—three position sensors; 6—two 250 W CO₂ lasers; 7—heating laser kill switch; 8—Vision Research model 9.1 camera; 9—Infinity long distance microscope lens; 10—Exactus pyrometer at back side of apparatus. A glowing levitated and laser beam-heated sample (11) is at the center.

and V-I phase differences in the amplifier circuits from which resonant frequencies and acoustic outputs are calculated. The operating frequency is automatically controlled to equal the average of the six resonant frequencies and the digital signal generator signals are controlled to maintain constant acoustic outputs. Resonant frequencies drift to lower values as the transducers warm up. On-off control of the transducer cooling fans makes the resonant frequencies drift to a common value, typically within a few Hz of the operating frequency.

The gas jet flow rate is controlled by a 0-5 liter/min MKS Type M100B flow control transducer and type 247D readout device. The gas jet assembly has position and tilt adjustments, and a heater with temperature capabilities to approximately 600 °C. Heating is used to increase viscosity of the gas and maintain laminar gas jet flow. The heater temperature control, item 3 in Figure 1 shows a 523 °C heater temperature, as measured with a chromel-alumel thermocouple. Height is typically adjusted to levitate a sample 2.5 cm above the exit of the 2.36 mm inside diameter mullite flow tube. Tilt is set to incline the gas jet by approximately 0.1° from vertical towards the Vision Research camera. Best control of sample rotation is obtained with this slight bias from vertical gas jet flow.

Sample position sensing is used for feedback control of acoustic forces to damp out fluctuations in the position of levitated samples. Perpendicular to each acoustic axis, a shadow

of the sample in the light from an 808 nm laser diode beam is imaged onto a Hamamatsu model S5991-01 two-dimensional position-sensitive detector. A narrow-band spectral filter, spatial filter, and 40 KHz modulation of the laser light are used to obtain position sensing with negligible interference from incandescent light, even at sample temperatures above 3000 °C.

Levitated samples are heated on opposite sides in the beams from two Synrad Evolution 240 CO₂ lasers. The laser beams pass through beam steering optics and ZnSe lens that can be adjusted to vary the intensity and size of the beam at the sample. Temperatures in excess of 3000 °C are obtained by heating oxide materials with less than the 250 W maximum output power of each CO₂ laser. The laser beams are slightly inclined so that the end surface of each beam delivery tube serves as a beam stop for the opposite laser.

An Infinity model K2SC long-distance microscope lens with model CF-2 objective and Phantom V9.1 camera from Vision Research, Inc. yield images with 14-bit image depth at up to 1000 fps (frames per second) at a full resolution of 1632 × 1200 pixels. The camera and lens produce near full-scale images for 3 mm diameter levitated samples. Imaging rates of 2600 Hz were obtained at a reduced resolution of 960 × 720 pixels.

The Exactus pyrometer is model EX-S-1PY-ECS from BASF Corporation. It detects light in a narrow waveband

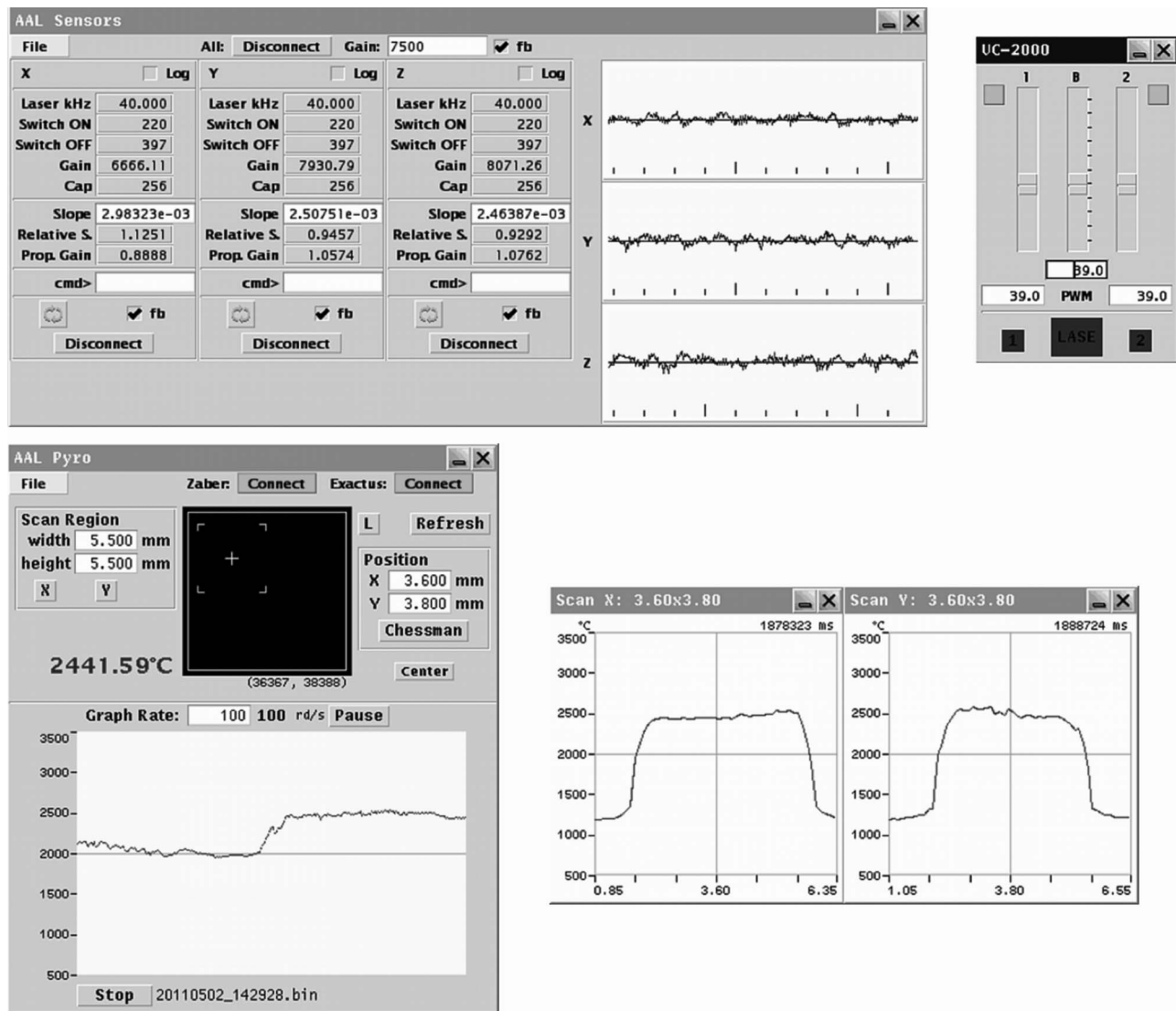


FIG. 2. Sensor screen (top left), laser power control screen (top right), and bottom-pyrometer control and X and Y pyrometer scan screens.

at 650 nm. The measurement spot size is less than 0.80 mm (99.9%) at an operating distance of 150 mm. Temperature measurement range is 580 °C to 3500 °C at rates up to 1000 Hz. The pyrometer is mounted on a Zaber LS13E Motorized X-Y stage with 13 mm travel per axis for obtaining temperature scans on levitated samples.

Samples are inserted in the levitated position with a vacuum chuck comprised of a ceramic tube connected to a small vacuum pump. The operator creates a vacuum to grip a sample at the end of the ceramic tube by placing a thumb over a hole in the opposite end of the tube. The tube is then inserted through a guide until the sample is centered as seen on the video monitor. The sample is released, the tube withdrawn, and levitation occurs if the gas flow is within a few percent of the appropriate value. Non-spherical samples are more readily levitated if laser beam heating begins just as they are released by the vacuum chuck.

A Perle Systems, Ltd. IOLAN model device server is installed in the system frame. It provides Ethernet connection to serial communication devices of the AAL system. Details

of the communication protocols, control electronics, and software have been described elsewhere.^{11,12}

B. Levitator controls

Levitation is stable when the acoustic and aerodynamic levitation forces balance the sample weight. Changes in these forces occur with sample temperature, shape, and position such that the levitated sample may become unstable if its position fluctuations are not damped out. The operators perform manual changes in the gas flow rate and in acoustic controls to maintain the levitated sample at the point where it intercepts the CO₂ laser heating beams. Fluctuations in the sample position are automatically damped by changes in the acoustic node positions in response to velocity feedback from the position sensors.

1. Position sensor, pyrometer, and laser power

The position sensors, laser power, and pyrometer screens of the computer control system are shown in Figure 2. The

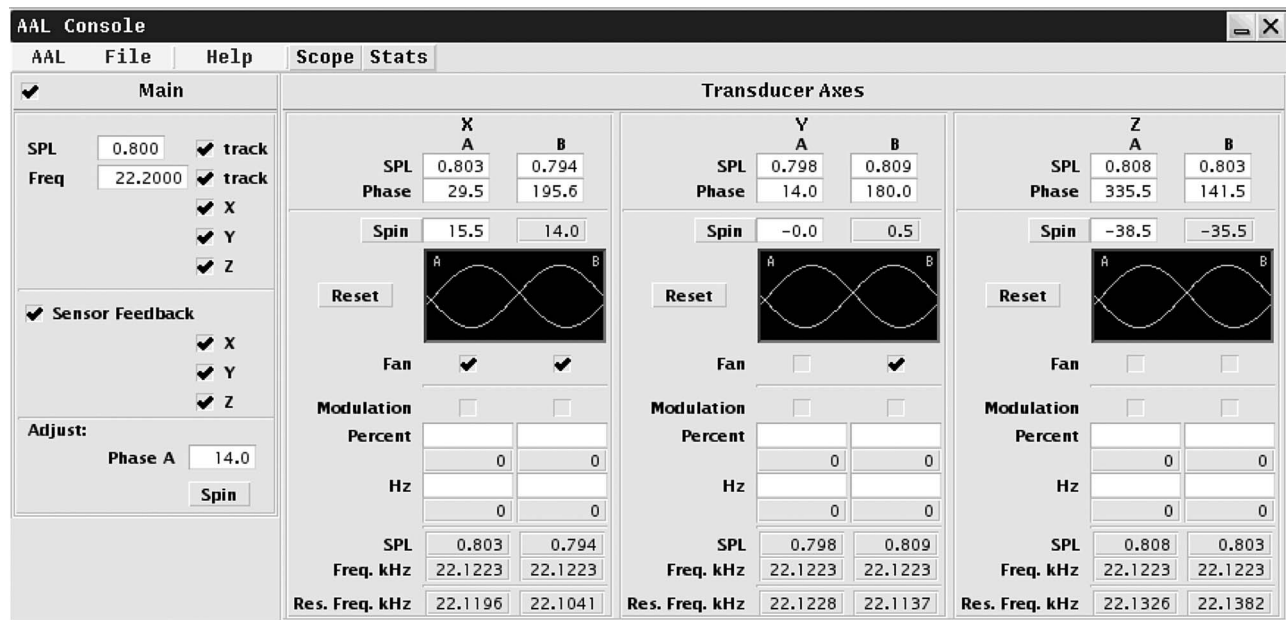


FIG. 3. Acoustic control screen.

sensors screen turns on feedback control of the sample position, sets the sensor gains, and plots 1 s of sample velocity measurements along each of the three acoustic axes. Sensor gain determines the magnitude of automatic changes to the acoustic phases that move the levitation node in response to a given sample velocity. If the “Log” boxes are checked on the screen, sample velocity measurements are recorded at a frequency of 250 Hz. On the sensors screen, “gain,” “slope,” and “relative sensitivity” are from calibration of sensor output vs the position of levitated samples for each axis. “Switch on/off” synchronize position sensing with the modulated sensing lasers. “Cap” places a maximum on the value of sample velocity that may be transmitted to the acoustic controls.

The laser power screen sets the percent of full-scale laser power. With the pointer on the percent indicator box (as shown in Figure 2), the keyboard up/down arrow or up/down page keys make 1% or 5% changes in the laser output power. Smaller changes can be manually entered from the keyboard.

The pyrometer control screen initiates horizontal (X) and vertical (Y) temperature scans of the sample surface. It sets and indicates the width and height and the pyrometer center position for the temperature scans, within the range of the pyrometer translators. The graph shows the most recent 1 min record of the measured temperature. The temperature measurement rate is set on the screen and the “start/stop” button at the bottom of the screen turns temperature recording on or off.

The pyrometer scan screens show the results of horizontal (X) and vertical (Y) temperature scans. The scans shown in Figure 2 determine the vertical and horizontal dimensions to be 3.42 mm and 4.07 mm, respectively, for the levitated molten oxide sample. The aspect ratio is determined primarily by the effects of gravity and surface tension, although shape changes due to acoustic squeezing can be obtained at increased acoustic pressures.

2. Acoustic control screen

The acoustic control screen (“AAL Console”) is shown in Figure 3. It has two panels labeled “Main” and “Transducer Axes.” The Main panel sets the acoustic frequency at start-up (in this case to 22.2000 KHz) and the acoustic intensity as sound pressure level (SPL). It turns frequency tracking, SPL control, and sensor feedback on or off. The acoustic operating frequency and transducer resonant frequencies are shown at the bottom of the Transducer Axes panel. In this case the operating frequency of 22.1223 KHz differs by 0.5 Hz from the average resonant frequency value for the six transducers. This difference and slight differences between the transducer and set values of SPL occur because the resonant frequency and acoustic outputs drift as the transducers warm-up during a 5 s period between each reset of frequency and amplifier power values.

The phase difference in the acoustic outputs for each set of the A and B transducers is automatically set at start-up to 180°. This places a node in the standing wave (where a sample is levitated) exactly halfway between opposed transducers if the acoustic medium is uniform, or if it has properties symmetrical about the center point. The transducers are aligned such that the acoustic axes meet at this center point where the center nodes for each axis overlap and samples are levitated. When a sample is heated, the acoustic medium becomes unsymmetrical. Gas temperatures are slightly higher, on average above the sample than below it. This temperature difference causes the central standing wave nodes to move downward. The nodes are restored to the center by changing phase differences to a value less than 180°. The change is made by clicking on the “Phase A” adjustment at the bottom part of the Main panel.

The “Spin” values shown on the acoustic control screen are a second set of transducer phase adjustments that control acoustic torques on a levitated sample. Experience showed

that rotation of a levitated sample was minimized if the phase of both members in each pair of transducers is changed by the amount given in the following equation:

$$\text{Spin}(\text{°}) = 2.1(F - F_{AB}) - 8. \quad (1)$$

F and F_{AB} , in Hz, are the operating acoustic frequency and the average resonant frequency of the two transducers for a given axis. The values obtained from this function are displayed on the acoustic control screen on the right side of the spin entry fields. The “Spin” values are automatically set to these values by clicking on the spin button at the bottom of the Main panel or individually for each axis by clicking axis spin buttons in the Transducer Axes panel. Further changes in the spin settings can be made by the operator based on sample rotation rates determined from recordings with the Vision Research camera. The rule for manual spin changes is based on the direction towards which the top of a levitated sample rotates. If the direction is towards the upper B-transducer of a particular acoustic axis, sample rotation will decrease if the spin setting for that axis is increased. The spin settings displayed on the left side of the spin entry fields in Figure 3 show small changes that were made by the operator from Eq. (1) values.

Cooling fans draw air through the acoustic transducers. The fans are automatically turned on or off if the operating frequency is greater than or less than the resonant frequency of a given transducer. This control makes the resonant frequency of all transducers drift towards the operating frequency as the transducers warm-up.

The acoustic control screen allows modulation of the acoustic amplitude for one or more of the transducers. This facility can be used to investigate shape oscillations of levitated liquid drops. The frequency range for acoustic intensity modulation is limited by the high Q values of the acoustic transducers, from 0 to approximately 200 Hz. At low frequencies, acoustic modulation allows the slow shape relaxation of viscous liquids to be observed. At higher frequencies, the natural oscillation frequencies and oscillation decay rates of low-viscosity liquids can be excited and measured to determine surface tension and viscosity, based on the theories of Rayleigh¹³ and Lamb.¹⁴

C. Experiments

1. Levitator operation

Experiments first characterized operation of the acoustic transducers to obtain calibration data used in the system’s operating software. The output of each acoustic transducer was measured with a calibrated 1/8” diameter Bruel & Kjaer (B&K) Model 4138 microphone as a function of the frequency, voltage, current, and current-voltage phase difference of the acoustic amplifier output. The decay rate of transducer output was measured with the microphone and a storage oscilloscope when the output of the acoustic amplifier was turned off. These results gave the functional relations between acoustic amplitude and the frequency, amplifier power, or time following a change in amplifier power. The transducer resonant frequency was determined along with the difference between the resonant and operating frequency as a function of the

current to voltage phase difference in the acoustic amplifier output.

The sensitivity of the position sensor outputs to levitated sample position was measured as follows. A Styrofoam bead was levitated by operating a single acoustic axis at an acoustic output sufficient to hold the bead close to the center of the central acoustic node. The phase of the acoustic output was then varied at one transducer while the phase of the opposed transducer was held constant. This resulted in a one-wavelength change in the node position as the phase difference varied from 0° to 360°. Taking the wavelength equal to 1.56 cm in air at ambient temperature at the nominal acoustic frequency of 22 200 Hz gave the sensor output vs sample position from the sensor output vs phase measurements.

Operation of the feedback control system for damping sample position fluctuations was demonstrated for purely acoustic levitation. A water drop was levitated and disturbed by a sharp knock on the system frame. Recording of the sensor velocity output on the sensor screen was promptly turned off to preserve the record of sample position fluctuations. The experiments gave the typical frequency of fluctuations and the rate at which fluctuating position was damped by controlling acoustic phase values in response to the sample velocity feedback signals.

Operation of the acoustic frequency control system was demonstrated. The transducers were operated at a typical output used in levitation experiments such that the resonant frequencies would decrease by some 50 Hz during transducer warm-up. The control system turned the cooling fan on or off if the transducer’s resonant frequency was less than or greater than the operating frequency. The operating frequency was controlled to equal the average resonant frequency of the six transducers.

The effect of laser-beam heating of a levitated sample on the acoustic and aerodynamic levitation forces was investigated in experiments with a levitated solid aluminum oxide sphere. Changes were made in the temperature of the laser-beam heated sphere and in the acoustic intensity and gas flow rate and position changes in the levitated sample were observed.

2. Modeling experiments

The Phase A value given in Figure 3 is 14.0°. This is the value determined for a levitated aluminum oxide sphere heated to a temperature of 1500 °C. The node location was found in the experiment by observing whether the levitated sphere moved up or down when the acoustic intensity was increased. Numerical modeling of the sound field was performed to investigate the influence of sample temperature, ambient temperature, and transducer spacing on the acoustic levitation forces.

3. Levitation experiments

A 3 mm diameter, 56 mg Al_2O_3 sphere (density = 4 g/cm³) was levitated at a nitrogen gas flow rate of 3.1 liter(stp)/min with a gas heater temperature of 540 °C. Based

TABLE I. Properties of processed materials.

Sample material	Melting point (K)	Density (g/cm ³)	Diameters (mm)
Al ₂ O ₃	2327	4.0	2.5–3.2
Y ₃ Al ₅ O ₁₂	2215	4.5	3.0
ZrSiO ₄	1960–2540	4.65	2.5–3.2
Y ₂ O ₃	2713	5.01	2.9–3.1
HfO ₂	≈3030	9.68	2.3–2.65

on the viscosity of nitrogen at 540 °C, these flow conditions correspond to a jet Reynolds number approximately 1300. The maximum flow rate, 5 liter/min was insufficient to levitate 3 mm diameter samples of HfO₂ (density = 9.6 g/cm³) but 2.5 mm HfO₂ samples were successfully levitated. Levitated mass increases in proportion to the momentum flow rate of the gas jet.

Laser beam heating and melting experiments were performed on Al₂O₃, HfO₂, Y₂O₃, Y₃Al₅O₁₂, and ZrSiO₄. Sample material melting points, densities, and diameters are given in Table I. The levitation process was extremely stable on laser heated and melted samples at temperatures up to approximately 2600 °C. Levitation was less stable at higher temperatures but experiments were performed with levitated molten Al₂O₃ at apparent temperature up to 3200 °C.

III. RESULTS

A. Levitator operation

Figure 4 shows the result for one transducer of acoustic output and amplifier electrical power as a function of the acoustic frequency. Acoustic output is taken as the “sound pressure level” or SPL. The acoustic output is proportional to the square root of electrical power as given by the product of the amplifier voltage V , current I , and cosine of the V – I phase difference ϕ .

The results in Figure 4 were obtained at a relatively small value for the amplifier power to minimize warm-up of the transducer and change in its resonant frequency during the

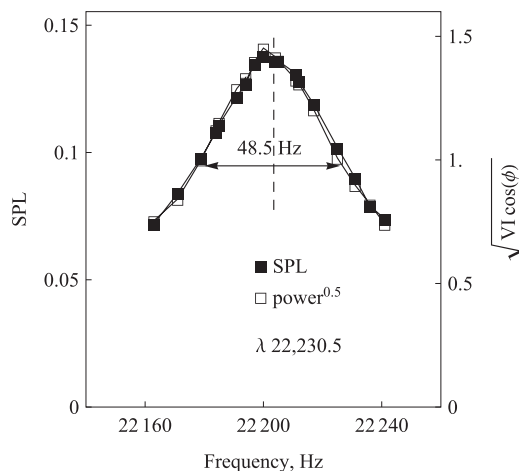


FIG. 4. Sound pressure level (SPL) and amplifier power output vs acoustic frequency, with maxima at the resonant frequency.

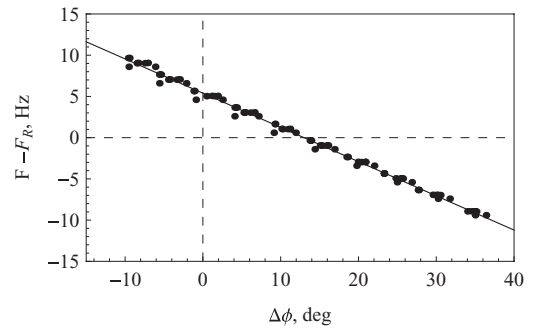


FIG. 5. Effect of off-resonant operation of an acoustic transducer on the current-voltage phase difference in the acoustic amplifier circuit.

experiment. A continued linear relationship between acoustic output and the square root of amplifier output power was demonstrated by measurements at a single frequency over a larger range of SPL values.

Figure 5 shows the difference between the operating frequency, F , and the resonant frequency of a transducer, F_R , as a function of the current-voltage phase difference in the acoustic amplifier circuit. The results are given for the relatively small, ± 10 Hz difference in frequencies that prevailed during levitation experiments. A linear analysis was sufficient within this range although the relationship becomes nonlinear at larger frequency differences.

Table II summarizes the results obtained on all six transducers. The values in row 1 of the table give the constant, A_{SPL} that determines SPL from the amplifier output power, P , as given in Eq. (2). The two constants, A_1 and A_0 in rows 2 and 3 of the table determine the difference between operating and resonant frequencies, $F - F_R$ from the current-voltage difference, $\Delta\phi$, as given in Eq. (3).

$$SPL = A_{SPL} \times \sqrt{VI \cos(\Delta\phi)}, \quad (2)$$

$$F - F_R = A_1 \Delta\phi + A_0. \quad (3)$$

Figure 6 shows the decay of acoustic power when the acoustic amplifier power was turned off. The decay time constant is $\tau = 7.6$ ms. Acoustic intensity modulation or phase change will be significantly damped at a frequency, $1/\tau = 132$ Hz, and highly damped at much greater modulation frequencies.

Figure 7 shows the relationship between the X-axis position sensor output and the position of an acoustically levitated Styrofoam ball. The position sensor signal is the quotient of two voltages, V_Y proportional to the position of the sample

TABLE II. Acoustic transducer calibration constants.

	XA	XB	YA	YB	ZA	ZB
A_{SPL}	0.1132	0.09092	0.11121	0.11202	0.11335	0.12008
A_1	-0.4526	-0.4754	-0.5050	-0.4615	-0.4603	-0.4334
A_0	7.121	6.760	8.613	6.213	6.255	5.949

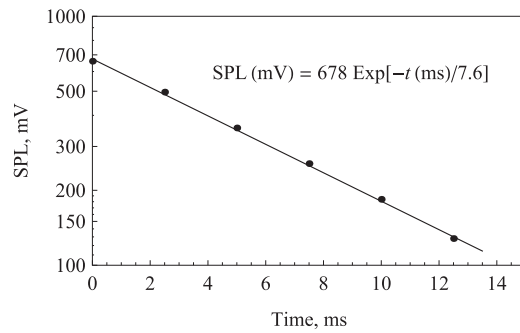


FIG. 6. Acoustic intensity decay when a transducer is turned off.

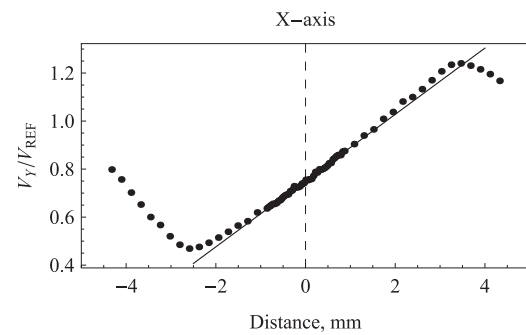


FIG. 7. Position detector signal vs position of an acoustically levitated sample.

shadow on the detector and V_{REF} proportional to the total detector intensity. The line is a least squares fit of data for phase differences of $\pm 38^\circ$, equivalent to a distance of ± 0.82 mm (at room temperature) and greater than typical fluctuations in the position of levitated samples. At larger distances from the center, the position signal goes through maximum and minimum values as the sample shadow passes the edges of the detector.

Figure 8 shows a test of the frequency control system. It plots the difference between the resonant and operating frequencies and the value of the operating frequency, F , during a 2-h period. The operating frequency decreased by 54.5 Hz during the experiment. The resonant frequency range of the six transducers was initially 18 Hz and decreased to 8 Hz with on/off control of the transducer cooling fans. The resonant frequency of three transducers, ZB, YA, and XB promptly drifted to precisely match the operating frequency.

Figure 9 shows the damping of position fluctuations of a levitated water drop. Quantities proportional to the velocity of motion are plotted on the vertical axes against time on the horizontal axis. The oscillation frequency is approximately 19 Hz and the damping time constant is approximately 0.2 s.

B. Acoustic field modeling

Assumptions used to model the standing wave behavior were (i) a one-dimensional sound field in air with temperature, T equal to the sample temperature, T_S , over a 3 mm sample distance and decreasing exponentially over a greater distance towards the upper, B, than the lower, A, transducer; (ii) an estimated 30% of the sound emitted by one transducer is back-reflected by the opposite transducer and contributes to the standing wave properties; and (iii) the effect of a heated gas jet was ignored—ambient temperature, T_A was taken equal to 300 K. The temperature field was thus modeled to equal the sample temperature over a distance equal to the sample diameter and be given on opposite sides of the sample by the following equation:

$$T - T_A = (T_S - T_A) \exp \left[-\frac{(z - z_S)^2}{2\sigma^2} \right]. \quad (4)$$

Here, z_S is the position of the upper or lower edges of the sample measured along the inclined axis of the transducer pair. The value of σ is smaller below than above the sample.

Figure 10 illustrates the predicted acoustic amplitudes for a sample temperature equal to 3000 K. The values $\sigma = 0.20$ cm above and $\sigma = 0.12$ cm below the sample

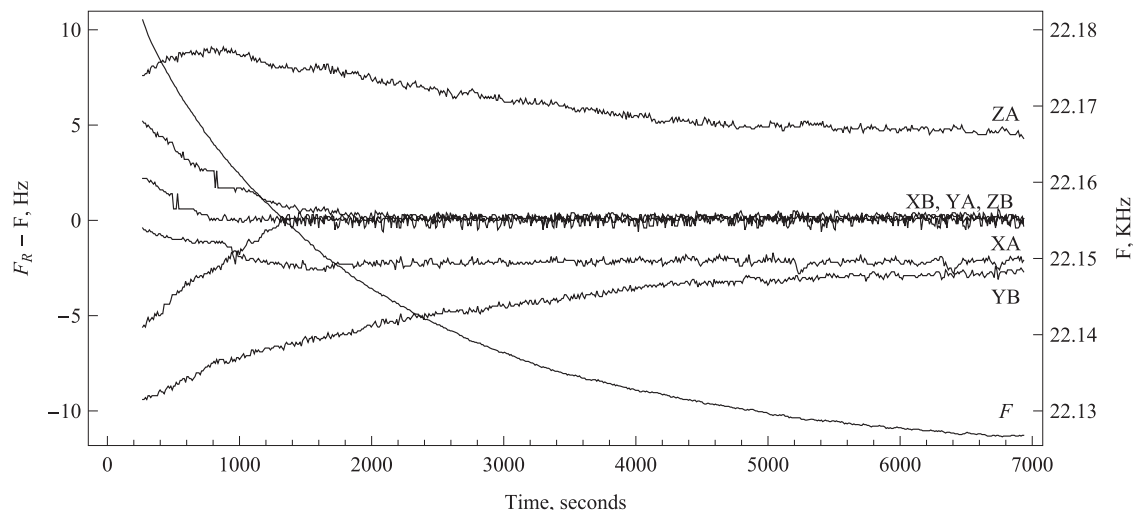


FIG. 8. Resonant frequency drift during warm up of the acoustic transducers.

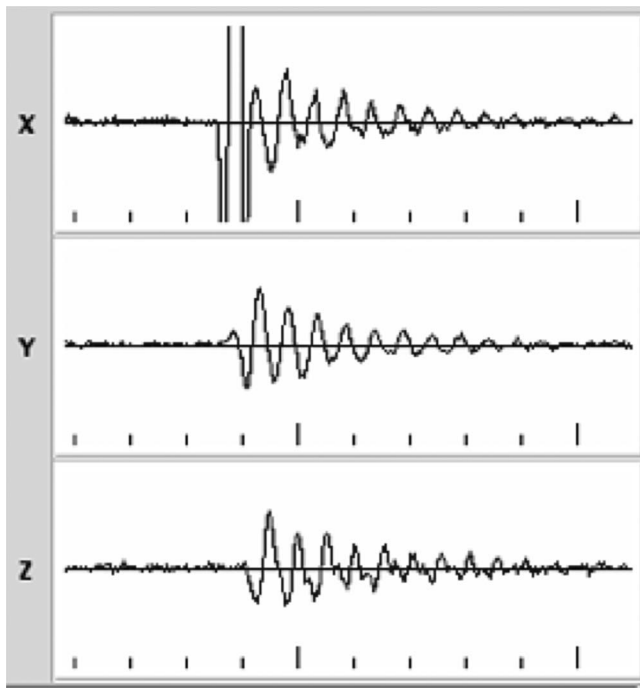


FIG. 9. Position sensor output vs time for a 1 s interval showing damped oscillation of an acoustically levitated water drop.

were used, and gave Phase A = 14.7° at $T_S = 1500^\circ\text{C}$, close to the observed value. Panel (a) is the result for the installed transducer spacing of 14.8 cm and sample levitation at 7.4 cm. Panel (b) is for a spacing of 15.48 cm with levitation at a slightly off-center position at 7.69 cm above the bottom transducer. For the as-installed case the value of Phase A is 14.1° . In the modified case, Panel (b), the transducer separation is taken equal to the value for a half-integral number of acoustic oscillations and the levitation position chosen at the off-center position of the central node with the 3000°C sample temperature, Phase A = 0, and the transducers operating 180° out-of-phase. This set-up yields in-phase contributions of the direct and reflected sound to the standing wave and maximizes the acoustic force at the given sample temperature.

Figure 11 illustrates the model values for the Phase A adjustment and the magnitude of the acoustic intensity gradient

at the central node for the two cases. The as-installed system exhibits a nearly constant Phase A value for sample temperatures above 1000 K. This is a convenient feature that eliminates the need to adjust Phase A with sample temperature. The alternate transducer positioning yields increased acoustic gradients at higher temperatures, at the expense of a much greater temperature dependence of Phase A. These differences are the result of positioning the transducers at a distance equal to a half-integral number of acoustic oscillations when the sample is near ambient temperature (as installed) or at 3000 K.

The model results illustrate phenomena to be considered in perfecting the levitator configuration. In practice, the optimum transducer spacing will depend on the ambient and sample temperatures, sample size and shape, levitation gas flow rate and composition, and differences between actual and the assumed model calculation conditions.

C. Levitation heating and melting experiments

1. General observations

Experience confirmed the result predicted in Figure 11(a) that the Phase A adjustment is insensitive to sample temperature above 1000 K for the as-installed transducer spacing. The levitated sample position was stable at temperatures above 1000 K during rapid changes in the sample temperature. Laser beam heating could be turned off to observe deep undercooling of a liquid followed by crystal nucleation and rapid crystallization, then back on to reheat and melt the levitated sample.¹⁵

Spherical samples were easily levitated but it was not possible to detect their spin and liquid drops were ejected by centrifugal forces in attempts to melt the sample. Partial melting by careful and brief heating to the melting point was used to produce asymmetric features on the sample. This allowed sample rotation to be observed from fast-camera recordings and eliminated with the spin adjustments. Highly non-spherical samples tended to oscillate in position when inserted for levitation and would become unstable within a few seconds. Good stability of such samples was obtained by immediate rapid heating to incandescence when the sample was released.

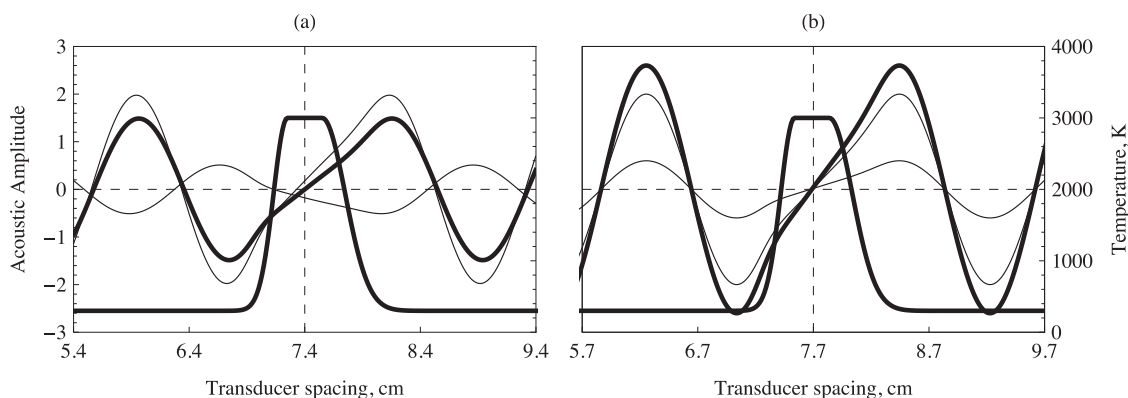


FIG. 10. Models of the acoustic sound field at maximum standing wave intensity for two sets of transducer positions. Lighter lines are contributions of the more-intense direct and less-intense reflected sound to the standing wave. Heavier lines are the total intensity of the standing wave and the temperature field.

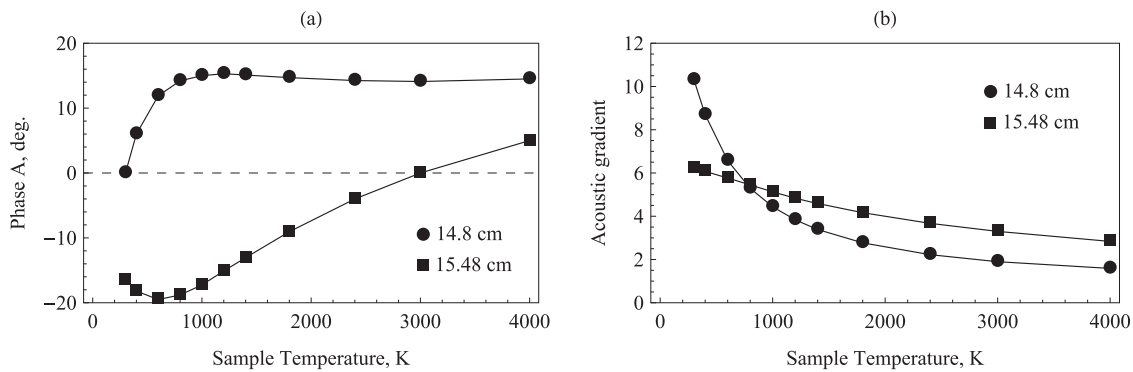


FIG. 11. Phase A and acoustic gradient values for two sets of transducer positions.

Melting was typically performed on a hot levitated sample by making a substantial increase in heating laser power. A decrease in laser power could then be made when complete melting was signaled by the temperature vs time measurements. The sample would remain molten even if the temperature thus decreased below the melting point. Levitation stability during melting was more easily maintained with congruently melting materials than for materials that melt over a large temperature range. Completely molten samples assumed a smooth and symmetrical liquid drop shape and were very stable at temperatures up to approximately 2600 °C. Levitation stability decreased at higher temperatures, but experiments with molten Al_2O_3 at apparent temperatures up to 3200 °C were possible. At such high temperatures, mass loss due to evaporation was rapid and Al_2O_3 smoke formed by condensation in the wake of the levitated sample. No discoloration of Al_2O_3 was observed after heating to 3200 °C in nitrogen. Al_2O_3 evaporation occurred at similar rates in nitrogen or in air.

The open structure of the levitator allowed well focused imaging of levitated samples. Photographs of molten and crystallizing samples obtained at a frequency of 2600 Hz with the Vision Research camera are given in Figure 12. In one case, an image of undercooled liquid Al_2O_3 was analyzed to determine the image edge locations. Regression fits of intensity vs pixel measurements determined the image width to be 634.83 ± 0.39 pixels. Increased precision in sample dimen-

sion measurements would be possible with precise focussing of the camera and use of higher resolution measurements at an imaging frequency no more than 1000 Hz.

2. Undercooled liquids

Undercooled liquids were maintained for extended periods of time under the containerless conditions. For example, the temperature vs time data in Figure 13 record liquid $\text{Y}_3\text{Al}_5\text{O}_{12}$ (YAG, yttrium aluminum garnet) maintained in an undercooled state for more than 18 min, including 6 min at a temperature more than 500 °C below the melting point. The inset in Figure 13 shows the increase in temperature (recalescence) near the end of the experiment due to the heat released by rapid crystallization when the temperature was decreased below the crystal nucleation temperature.

Crystal nucleation and recalescence results are given in Table III for YAG, Al_2O_3 , and Y_2O_3 . Initial temperatures were greater than the melting points except for the case illustrated in Figure 13. The nucleation and recalescence temperatures were highly reproducible but dependent in some cases on the levitation gas or the initial temperature. Cooling of molten YAG gave three different results including rapid crystallization nucleated at $T_a \approx 1145$ °C, slow crystallization nucleated at $T_a \approx 883$ °C, and not shown in Table III, the absence of crystallization and formation of a glass product.

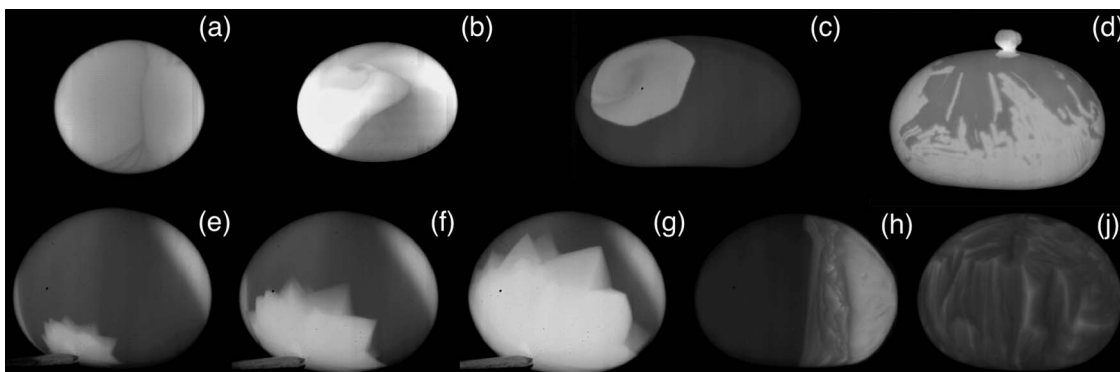


FIG. 12. Levitated and melt processed materials. (a) Liquid Al_2O_3 at $T_a \approx 3200$ °C, (b) liquid HfO_2 at $T_a \approx 2910$ °C, (c) undercooled liquid Y_2O_3 at the instant of crystal nucleation, (d) solid Y_2O_3 during the hexagonal to cubic phase transition at 2326 °C,¹⁶ (e)-(g) crystal propagation in undercooled liquid Al_2O_3 initiated by an iridium stinger, (h) partially crystallized $\text{Y}_3\text{Al}_5\text{O}_{12}$ in the deeply undercooled liquid at $T_a \approx 1200$ °C, (j) crystallizing $\text{Y}_3\text{Al}_5\text{O}_{12}$ viewed through the transparent liquid.

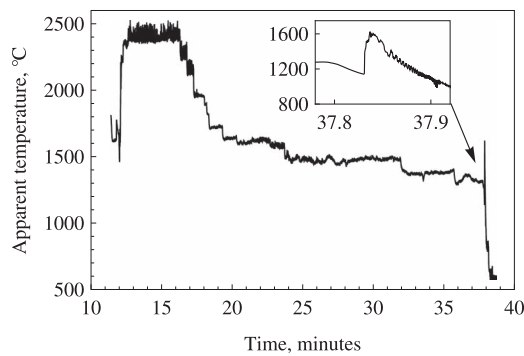


FIG. 13. Temperature vs time measurements for an experiment with undercooled YAG. The liquid is undercooled at apparent temperatures below approximately 1930 °C.

3. High temperature stability

Figures 12(a) and 12(b) are images of levitated molten Al_2O_3 and HfO_2 at respective apparent temperatures of 3200 °C and 2910 °C. These photographs were obtained in experiments that achieved the high temperatures but also produced levitation instability that caused fluctuations in the sample temperature. Even so, molten Al_2O_3 was maintained at apparent temperatures above 2700 °C for 3.5 min including 68 s above 2900 °C.

Levitated samples were stable and temperatures were easily maintained within ± 10 °C at temperatures up to 2500 °C. Temperature control deteriorated at higher temperatures as decreasing levitation stability caused fluctuations in the laser heating power. The temperature stability vs temperature recorded in several experiments with Y_2O_3 and Al_2O_3 is illustrated in Figure 14. The smaller values of the temperature fluctuations that are given in the figure are from experiments in which more care and time was taken to stabilize the sample levitation.

4. Y_2O_3

Figures 12(c) and 12(d) show images of a levitated Y_2O_3 sample obtained at a video frequency of 2600 Hz. Figure 12(c) is the first image obtained after crystal nucleation in a rapid cooling experiment. The bright region is the area heated by the initial crystallization. Figure 12(d) was obtained 40 ms later after crystallization was complete, during the hexagonal to cubic phase transformation¹⁶ of Y_2O_3 at

TABLE III. Initial, nucleation, and recalescence temperatures.

Material	Process	Expt.	Gas	Apparent temperatures (°C)		
				Initial	Nucleation	Recalescence
YAG	Rapid cooling	1	N_2	2230	1140	1684
YAG	Slow cooling	1	N_2	1280	1150	1622
YAG	Rapid cooling	1	N_2	2000	883	1234
Al_2O_3	Rapid cooling	9	N_2	2434 ± 39	1613 ± 4	1974 ± 4
Al_2O_3	Rapid cooling ¹⁵	9	Air	2217 ± 38	1707 ± 14	2000 ± 2
Y_2O_3	Rapid cooling	4	N_2	2634 ± 44	2101 ± 20	2361 ± 10
Y_2O_3	Rapid cooling	3	Air	2616 ± 27	2091 ± 22	2364 ± 23

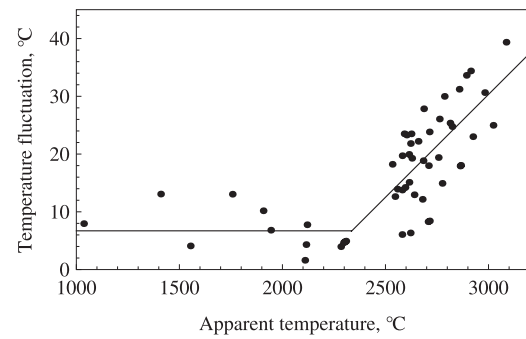


FIG. 14. Sample temperature fluctuations.

2326 °C. Bright regions of the image are the growing cubic Y_2O_3 crystals.

The cooling curve observed when laser beam-heating of molten Y_2O_3 was turned off is given in Figure 15. The sample was levitated in a stream of nitrogen gas. The liquid cooled from a temperature approximately 250 °C above to 250 °C below the melting point in 0.35 s and crystallized spontaneously within 2 ms. It then cooled below the crystal phase transition temperature, was reheated to the phase transition temperature and continued to cool after the transition was complete. A nearly identical cooling curve was observed for levitation in a stream of dry air¹⁵ with nucleation and recalescence temperatures as given in Table III.

5. Al_2O_3

Figures 12(e)–12(g) show 3 images at intervals of 0.77 ms of crystals growing in undercooled liquid aluminum oxide levitated in a nitrogen gas stream. In this experiment the heating laser power was reduced to cool the liquid below the melting point and crystallization was initiated by contact with an iridium metal wire “stinger” at an apparent temperature equal to 1857 °C. The figures show growing crystal dendrites that rapidly heated the liquid to the melting point where crystallization continued more slowly.

Images obtained when using the stinger to initiate crystallization allowed the rate of crystal growth in the undercooled liquid to be determined as a function temperature. The results are shown in Figure 16 as a plot of crystallization rate vs reciprocal temperature. In making this plot emissivity

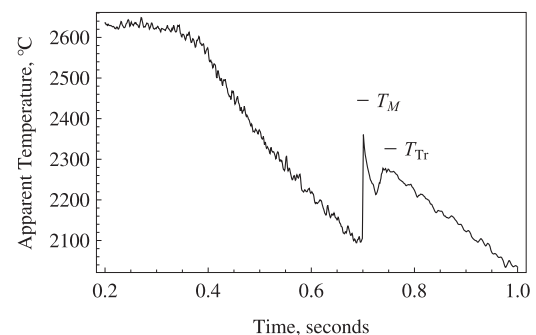


FIG. 15. Y_2O_3 cooling curve with crystallization of undercooled liquid followed by the hexagonal to cubic phase transition. True temperatures¹⁶ are marked for the melting point, T_M , and phase transition, T_{Tr} .

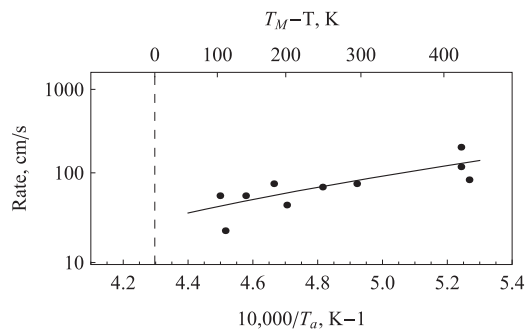


FIG. 16. Crystallization rate of undercooled liquid Al_2O_3 . The dashed line is at the melting point.

corrections to all of the apparent temperatures were made using the 0.93 value of the spectral emissivity of liquid Al_2O_3 at the melting point.¹⁷ The line drawn through the data is given by the equation:

$$\text{Rate} = 0.082 \exp\left[\frac{13700}{T}\right] \text{ cm/s.} \quad (5)$$

When molten aluminum oxide was cooled rapidly from a temperature above the melting point, crystals nucleated at $1613 \pm 4^\circ\text{C}$ for samples levitated in a nitrogen gas jet and at $1707 \pm 14^\circ\text{C}$ when levitated in air.¹⁵ These results agree well with previous measurements⁵ of spontaneous nucleation in liquid Al_2O_3 , with the nucleation temperature in nitrogen comparable to the value previously measured in an argon gas flow. The spectral absorption coefficient of liquid Al_2O_3 is smaller in an inert gas than in air.¹⁸ Therefore, the difference in apparent values of the nucleation temperature may be due to differences in liquid transparency rather than differences in the true temperatures at which spontaneous nucleation occurs. Transparency will also be responsible for increasing errors in the temperature values used in Figure 16 with a decreasing liquid temperature.

6. $\text{Y}_3\text{Al}_5\text{O}_{12}$

Figures 12(h) and 12(j) show deeply undercooled $\text{Y}_3\text{Al}_5\text{O}_{12}$ samples during crystallization at $T_a \approx 1200^\circ\text{C}$ after crystal nucleation at $T_a = 883^\circ\text{C}$, far below the 1942°C melting point. During this experiment, the sample was levitated in a nitrogen gas stream and it rotated about a vertical axis at a frequency of 5.4 Hz. Figure 12(h) shows the sample oriented with crystalline material to the right side and transparent liquid to the left. Figure 12(j), obtained after the sample had rotated another 90° , shows the growing crystal surface as seen through the transparent liquid. Since the liquid has become transparent, the true nucleation temperature will be considerably greater than the apparent value.

This is the first observation of the slow crystallization of undercooled liquid $\text{Y}_3\text{Al}_5\text{O}_{12}$. In previous work¹⁹ glass formation and rapid crystallization following crystal nucleation at approximately 1300°C were observed in containerless processing of molten YAG. These effects were also seen in the present work, as illustrated in the cooling curves of Figure 17 obtained when the heating lasers were turned off. The figure

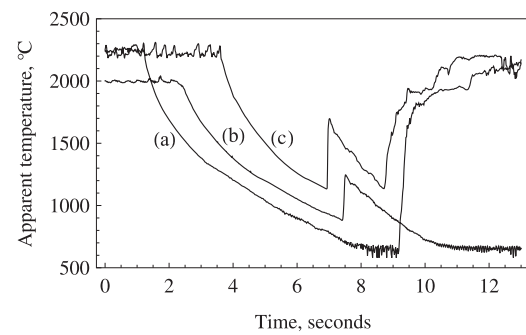


FIG. 17. Three different results obtained during undercooling of molten YAG. (a) Glass formation, (b) slow crystallization nucleated at $T_a \approx 895^\circ\text{C}$, and (c) fast crystallization nucleated at $T_a \approx 1140^\circ\text{C}$.

shows glass formation in curve (a) the slow crystallization in curve (b) and rapid crystallization in curve (c).

7. ZrSiO_4

When molten ZrSiO_4 levitated in air was held at apparent temperatures above 2400°C , rapid evaporation of silica produced ZrO_2 -rich liquids and recalescence as ZrO_2 spontaneously crystallized from the liquid. Temperature vs time behavior near the recalescence events is shown for two experiments in Figure 18. Precipitation of ZrO_2 produced a partially molten product for which levitation was not stable and failed promptly after the recalescence events.

Temperature measurements at the nucleation and recalescence events were interpreted as follows. The refractive index of the sample, $N(\lambda)$ was assumed equal to 2.0 at the pyrometer wavelength, $\lambda = 650 \text{ nm}$ where the images indicate that the liquid is opaque. The normal spectral reflectivity $r(\lambda)$ and emissivity, $\varepsilon(\lambda)$ are then given by the equation:

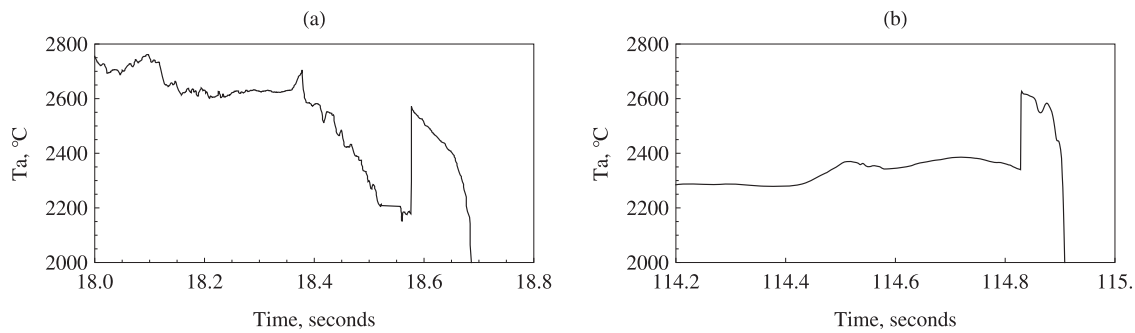
$$\varepsilon(\lambda) = 1 - r(\lambda) = 1 - \left(\frac{N-1}{N+1}\right)^2. \quad (6)$$

A value of 0.89 was thus estimated for the emissivity and used to correct apparent temperatures measured with the pyrometer to the true temperatures given in Table IV.

Figure 19 plots the approximate temperature vs composition path followed in the ZrO_2 - SiO_2 phase diagram²⁰ during the evaporation of silica, nucleation of ZrO_2 crystals, and recalescence processes. The paths are calculated assuming that recalescence yields the liquidus temperature. This assumption is consistent with the magnitude of the fusion enthalpy of ZrO_2 , 87 KJ/mol, and the heat capacity of crystalline ZrO_2 , 74.5 J/mol $^\circ\text{C}$, at the melting point²¹ Crystallization of less

TABLE IV. Nucleation and recalescence temperatures for zirconia-silica liquids.

Expt.	Apparent temperatures ($^\circ\text{C}$)		True temperatures ($^\circ\text{C}$)	
	Nucleation	Recalescence	Nucleation	Recalescence
(a)	2178	2555	2210	2598
(b)	2340	2616	2377	2661

FIG. 18. Recalescence events during evaporation of SiO₂ from molten ZrSiO₄.

than half the ZrO₂ content in the melts would be sufficient to yield the liquidus temperature.

IV. DISCUSSION

A. Levitation stability

Ambient temperature control is required to obtain best control of levitation conditions because the levitation force varies as the direct and reflected sound waves go in and out of phase with changes in the ambient temperature. The ideal situation has a transducer spacing equal to a half-integral number of wavelengths, which keeps reflected and direct sound waves in-phase. This can be done at all ambient and sample temperatures only if transducer spacing can be varied. Or if the ambient temperature is controlled, a fixed spacing can be chosen to optimize operation within the sample temperature range of interest.

The decreasing levitation stability above 2600 °C that is illustrated in Figure 14 is due in part to an increasing acoustic wavelength with temperature. At given acoustic amplitude, the force on a levitated sample decreases with wavelength as illustrated in Figure 11(b). This may be a relatively unimportant factor, since increasing the acoustic intensity has little influence on stability at the highest temperatures. A second effect is that with a phase difference between direct and reflected sound waves, the node location varies slightly throughout each acoustic cycle. This effect increases with wavelength and varies as sample temperature influences the phase difference. The effect on stability is not known, but could be investigated by changing the ambient room temperature or the transducer spacing.

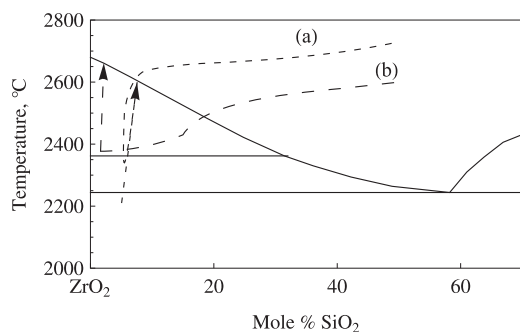


FIG. 19. Process model for experiments (a) and (b) shown in Fig. 18.

The increasing wavelength with temperature also influences the feedback loop that operates to reduce fluctuations in the sample position. Feedback control adjusts the position of the acoustic nodes formed by each pair of transducers to oppose motion of the sample, by changing the acoustic phase difference between the opposed transducers. The node motion resulting from a given sample position fluctuation is proportional to wavelength, and above 2600 °C is more than 3 times that at ambient temperature. Therefore, increasing sample temperature may make the feedback loop less effective in controlling fluctuations in the sample position. This possibility could be addressed by changes to the feedback software.

B. Sample oscillation in the acoustic well

In Figure 9, an acoustically levitated water drop is seen to oscillate in the acoustic well at a frequency of approximately 19 Hz. The oscillation frequency is explained as follows. We assume harmonic motion at a frequency, f , given by

$$f = \frac{1}{2\pi} \sqrt{\frac{k}{m}}. \quad (7)$$

In acoustic levitation the upward force at the bottom of the sample exceeds the sample weight by an amount equal to the downward force at the top of the sample. Taking the distance equal to the sample diameter and the force difference greater than the sample weight by a factor, F , we have

$$k = F \frac{mg}{d}, \quad (8)$$

$$f = \frac{1}{2\pi} \sqrt{F \frac{g}{d}}. \quad (9)$$

With a typical levitated water drop diameter of 0.25 cm, $g = 980 \text{ cm/s}^2$ and estimating $F = 2$, one obtains $f \approx 14 \text{ Hz}$, in reasonable agreement with the experimental result. A smaller frequency occurs in aero acoustic levitation because levitation is primarily by the aerodynamic force and the acoustic forces are smaller than the sample weight.

C. Nucleation temperature of Y₂O₃

Masuno *et al.*²² report a cooling curve, in air, for molten Y₂O₃ obtained under containerless conditions with a conical

nozzle-type of aerodynamic levitator. Their cooling curve is qualitatively similar to the present result in Figure 15 but differs in the magnitude of the two recalescence events. We find the temperature increase during recalescences by 280 °C and 60 °C compared with 78 °C and 38 °C in the previous work. We are confident in the accuracy of the present temperature measurements because they agree well with earlier⁵ nucleation and recalescence results on Al₂O₃ that were also obtained by aero acoustic levitation.

The present results on Y₃Al₅O₁₂ also yield nucleation temperatures less than the values obtained by the conical nozzle levitation technique.^{23,24} This difference is likely due to larger sample temperature gradients in the conical nozzle experiments than in the present work. Intense convective cooling occurs at the bottom part of samples levitated in a conical nozzle, where nucleation may occur at a temperature below the values measured by pyrometry at the upper part of the sample. This is a likely reason for the differences in Y₂O₃ nucleation temperatures found here and by Masuno *et al.*²²

The nucleation and recalescence results for Y₂O₃ are practically identical when measured using nitrogen or air¹⁵ for the levitation gas. No discoloration of the Y₂O₃ was observed when levitated and melted in nitrogen. Thus there is no evidence in the sample color or the cooling curve results for the substoichiometry of Y₂O₃ at high temperatures and low oxygen pressures reported by Ackerman and Thorn²⁵ and Krishnan *et al.*²⁶ It is possible that some oxygen is lost and replaced with nitrogen when Y₂O₃ is melted in nitrogen. Levitation in an argon gas flow with an added inert “shield gas” flow¹⁰ would yield very small oxygen and nitrogen partial pressures in studies of substoichiometry in molten oxides.

D. Absolute temperature measurement

Non-contact optical or infrared radiation pyrometry is the common method for temperature measurement in containerless experiments. A true temperature of the sample is determined only if the spectral emissivity is known over the spectral bandwidth of the pyrometer. Optical property data^{17,18} for Al₂O₃ suggest that relatively accurate emissivity values for liquid oxides can be obtained if the liquid is opaque and optical properties are known for the crystalline materials.

The spectral absorption coefficient,¹⁸ a_λ , of liquid Al₂O₃, at the melting point for a wavelength of 650 nm is 9 cm⁻¹ in argon and 41 cm⁻¹ in oxygen. The extinction coefficient, k_λ , given by

$$k_\lambda = \frac{\lambda}{4\pi} a_\lambda \quad (10)$$

is negligible so that normal spectral emissivity, ε_λ can be calculated from the refractive index, n_λ with Eq. (6).

The refractive index¹⁷ of liquid Al₂O₃ is 1.74, 5% less than the index for sapphire at the melting point and 2% less than the value of sapphire at room temperature. Thus, if an oxide melt is known to be opaque, quite accurate values for the index of liquid oxides can be estimated and emissivity calculated from Eq. (6) if the refractive index is known for

the solid phase. Refractive index values for many solid oxides are presently available at <http://refractiveindex.info/>.

This conclusion will not hold for deeply undercooled materials, because the absorption coefficient decreases with decreasing temperature. Figure 12(h) reveals the transparency of undercooled liquid Y₃Al₅O₁₂ and transparency in undercooled liquid Al₂O₃ is evident by the dendritic growth of crystals that can be seen within the liquid in Figs. 12(e)–12(g).

V. CONCLUSION

Advances in levitation technology have enabled several new experiments. This research demonstrated the ability to hold an undercooled oxide liquid for several minutes at temperatures far below the melting point. It allowed crystallization rates to be measured as a function of temperature in undercooled liquids. It achieved contamination-free experiments on liquids at temperatures up to 3200 °C.

Further improvements in the levitation technology are possible. Levitation stability at temperatures above 2600 °C may be obtained by optimizing position-sensing feedback control of acoustic forces. It will be possible with changes in software to automatically adjust the position sensing feedback control parameters to compensate for increased acoustic wavelength with sample temperature. Automatic control of acoustic transducer positioning can be developed to maintain in-phase contributions to the acoustic forces from direct and reflected sound. Application to air-sensitive materials can be made with an inert shield gas¹⁰ flow that prevents oxidation of levitated materials.

The open structure of an aero-acoustic and levitator facilitates its use for imaging and the use of optical techniques for property measurements on high temperature liquids. Ellipsometry can be used to measure liquid optical properties¹⁷ and obtain emissivity values needed to determine true sample temperatures. In fact, levitated liquids are ideal candidates for ellipsometry. Their smooth curved surfaces yield specular reflection over a range of angles that automatically includes the ellipsometric angle.

An improved “stinger” device for inducing the crystallization of undercooled liquids could be used to obtain accurate melting and liquidus temperatures. The method is that of Anderson,²⁷ in which the sample temperature is determined above which stinging fails and below which stinging succeeds in causing crystallization. For such work, the effect of residual temperature gradients in levitated samples can be eliminated if the video camera, stinger, and pyrometer are placed on the same side of the levitated sample.

It should be possible to develop accurate calorimetric measurements by using a capture device to carry a levitated sample into a calorimeter. Since rapidly cooled samples often yield non-equilibrium products, the heat measured in a “capture” calorimeter will not give a final result. One way to complete the calorimetric measurement is seen in the work of Tangeman *et al.*²⁸ who used high temperature solution calorimetry to measure the crystallization enthalpy of vitreous Forsterite, Mg₂SiO₄, formed in containerless processing experiments.

ACKNOWLEDGMENTS

The project was supported by the Deutsche Forschungsgemeinschaft (German Research Association, DFG) under the title “Bestimmung der Liquidus- und Solidusflächen im Dreistoffsystem $\text{Al}_2\text{O}_3\text{-ZrO}_2\text{-SiO}_2$ durch tiegel-freies Levitationsschmelzen,” Grant No. Te146/37-1, and “Schwebeschmelzanlage,” Grant No. GZ Inst 222/779-1 FUGG AOBJ: 544260, which is gratefully acknowledged.

- ¹J. K. R. Weber, D. S. Hampton, D. R. Merkley, C. A. Rey, M. M. Zatarski, and P. C. Nordine, *Rev. Sci. Instrum.* **65**, 456 (1994).
- ²J. K. R. Weber, J. J. Felten, B. Cho, and P. C. Nordine, *J. Jpn. Soc. Microgravity Appl.* **13**, 27 (1996).
- ³J. K. R. Weber, D. R. Merkley, C. D. Anderson, P. C. Nordine, C. S. Ray, and D. E. Day, *J. Am. Ceram. Soc.* **76**(9), 2139 (1993).
- ⁴J. K. R. Weber, J. J. Felten, B. Cho, and P. C. Nordine, *Nature (London)* **393**, 769 (1998).
- ⁵J. K. R. Weber, C. D. Anderson, D. R. Merkley, and P. C. Nordine, *J. Am. Ceram. Soc.* **78**, 577 (1995).
- ⁶K. Nagashio and K. Kuribayashi, *J. Am. Ceram. Soc.* **85**, 2550 (2002).
- ⁷K. Nagashio, K. Kuribayashi, and Y. Shiohara, *Acta Mater.* **49**, 2557 (2001).
- ⁸A. B. Biswas, J. K. R. Weber, and P. C. Nordine, *J. Mater. Res.* **10**, 1823 (1995).
- ⁹K. Nagashio, W. H. Hofmeister, D. E. Gustafson, A. Altgilbers, R. J. Bayuzick, and K. Kuribayashi, *J. Mater. Res.* **16**, 138 (2001).
- ¹⁰R. F. Cooper, J. B. Faselow, J. K. R. Weber, D. R. Merkley, and D. B. Poker, *Science* **274**, 1173 (1996).
- ¹¹J. A. SICKEL and P. Nordine, in *Proceedings of The 5th International Workshop on Plan 9*, <http://5e.iwp9.org/iwp95e.pdf>, p. 42.
- ¹²J. A. SICKEL, in *Proceedings of the 6th International Workshop on Plan 9*, edited by F. J. Ballesteros, E. S. Salvador, and G. G. Muzquiz (Universidad Rey Juan Carlos, Madrid, Spain, 2011), p. 45.
- ¹³J. W. S. Rayleigh, *Proc. R. Soc. London* **29**, 71 (1879).
- ¹⁴H. Lamb, *Proc. London Math. Soc.* **13**, 51 (1881).
- ¹⁵R. Telle, A. Kaiser, and P. C. Nordine, “Characterization of non-metallic melts by aero acoustic levitation,” in *Proceedings of the 12th Biennial Worldwide Conference on Refractories 2011*, Kyoto, Japan, 2011 (Curran Associates, Red Hook, NY, 2011), p. 357.
- ¹⁶D. Djurovic, M. Zinkevich, and F. Aldinger, *Calphad* **31**, 560–566 (2007); H. Okamoto, *J. Phase Equilib. Diffus.* **32**, 574 (2011).
- ¹⁷Krishnan, S., J. K. R. Weber, R. A. Schifman, P. C. Nordine, and R. A. Reed, *J. Am. Ceram. Soc.* **74**, 881 (1991).
- ¹⁸J. K. R. Weber, S. Krishnan, C. D. Anderson, and P. C. Nordine, *J. Am. Ceram. Soc.* **78**, 583 (1995).
- ¹⁹J. P. Coutures, J. C. Rifflet, D. Billard, and P. Coutures, in *Proceedings of the 6th European Symposium on Materials Sciences Under Microgravity Conditions, Bordeaux, France* (European Space Agency, 1986), pp. 427–30.
- ²⁰A. Kaiser, M. Lobert, and R. Telle, *J. Eur. Ceram. Soc.* **28**, 2199 (2008).
- ²¹M. W. Chase, Jr. *et al.*, JANAF Thermochemical Tables, 3rd ed. *J. Phys. Chem. Ref. Data* **14**, 1692 (1985).
- ²²A. Masuno, Y. Arai, and J. Yu, *Phase Transitions* **81**, 553 (2008).
- ²³J. K. R. Weber, J. G. Abadie, A. D. Hixson, P. C. Nordine, and G. A. Jer-man, *J. Am. Ceram. Soc.* **83**, 1868 (2000).
- ²⁴P. C. Nordine, J. K. R. Weber, and J. G. Abadie, *Pure Appl. Chem.* **72**, 2127 (2000).
- ²⁵R. J. Ackermann and R. J. Thorn, in *Science of Ceramics*, edited by G. H. Stewart (Academic, New York, 1961), pp. 397–406.
- ²⁶S. Krishnan, S. Ansell, and D. L. Price, *J. Am. Ceram. Soc.* **81**, 1967 (1998).
- ²⁷C. D. Anderson, W. H. Hofmeister, and R. J. Bayuzick, *Metall. Trans. A* **24**, 61 (1993).
- ²⁸J. A. Tangeman, B. L. Phillips, A. Navrotsky, J. K. R. Weber, A. D. Hixson, and T. S. Key, *Geophys. Res. Lett.* **28**, 2517, doi:10.1029/2000GL012222 (2001).